IEEE Access
Multidisciplinary | Rapid Review | Open Access Journal

Received November 20, 2019, accepted December 6, 2019, date of publication December 13, 2019,
date of current version January 14, 2020.

Digital Object Identifier 10.1109/ACCESS.2019.2959378

A Wideband Dual-Polarized Antenna and Its Array With Electrically Downtilt Function for 5G Sub-6 GHz Communication Applications

HAO JIN[1], LIJIA ZHU[2], HUANQING ZOU[1], YONG LUO[1], SHUGONG XU[1], (Fellow, IEEE), AND GUANGLI YANG[1], (Member, IEEE)

[1]Shanghai Institute for Advanced Communication and Data Science, Shanghai University, Shanghai 200444, China
[2]Key Laboratory of Specialty Fiber Optics and Optical Access Network, Shanghai University, Shanghai 200072, China

Corresponding author: Guangli Yang (guangli.yang@shu.edu.cn)

This work was supported by the Shanghai "Eastern Scholarship."

ABSTRACT A wideband dual-polarized antenna is proposed for 4G and 5G communication applications. The antenna element consists of a pair of opened-loop dipoles for dual-polarization and its three inherent resonant modes are shifted closer to form a wide bandwidth. With additional U-shaped slots etched around the feed point, the input impedance of the antenna element is matched to 50 Ohm. The fabricated antenna element operates from 1.8 to 4.0 GHz, having 75.9% (VSWR ≤ 2) impedance bandwidth and high port-to-port isolation (> 25 dB). It also achieves a $67\pm1°$ beamwidth in H-plane and $68.7 \pm 3.3°$ in V-plane with 8.5 ± 1 dBi gain across the supported bands. By using six antenna elements and designing RF phase shifting module (RFPSM) based on vector modulators, a six-element dual-polarized array with electrically downtilt is also fabricated and measured, realizing a peak gain of 16.8 dBi, a similar beamwidth in H-plane as single antenna element and an electrically downtilt in V-plane from 0° to 12° which is preferred in communication applications. This antenna array could be used for future 5G communication and other applications.

INDEX TERMS Wideband, dual-polarized, electrically downtilt, opened-loop dipoles, 5G.

I. INTRODUCTION

In the 5G era, massive mobile devices and access points need to be connected to the wireless network with fast data rate and channel capacity. The modern wireless communication system needs to support much more frequency bands than 4G. Also, due to the advantages of dual polarization to combate the multipath fading and reduce the number of antennas, dual-polarized antennas with wider bandwidth and stable radiation patterns are popular in communication applications. Additionally, to have better area coverage, the antennas with electrically downtilt from 0° to 12° are preferred, which means a cost-effective and well-performed RF phase shifting circuit also needs to be designed.

In terms of the antenna element design, cross dipoles are the most popular way to realize dual-polarization and high port-to-port isolation. Dipoles can be designed with different shape and size [1]–[7], such as fan-shaped dipoles [1], loop dipoles [2]–[5], and diamond-shaped dipoles [6], [7]. The dipoles usually have two resonant modes, the first mode is determined by the size of dipoles, and the second is the high-order resonant mode. Because two resonant frequencies are far apart in the spectrum, the dipoles in [1]–[3] only support narrow bandwidth from about 1.6 to 2.2 GHz. To combine two resonant modes to enhance bandwidth, parasitic cells, like fans [1], straight lines [2] and closed loop [3], are added between cross dipoles. After adding the cells, the second mode moves towards low frequency and combines with the first mode to achieve a wide bandwidth from about 1.7 to 2.8 GHz. In addition, some researchers adopt coupling feeding structures [4], [5] and balun-feeding structure [6], [7] to get a similar frequency coverage. To increase antenna bandwidth further, the dipoles in [4]–[7] add additional resonant structures like independent loops [4] embedded loops [5], closed slots [6] and vertically parasitic patch [7] to create additional third resonant mode at high frequency. However, due to the narrow bandwidth of the third resonant mode, the above dipoles can only cover the maximum bandwidth from 1.64 to 3.13 GHz, which is not enough to meet the requirements of next 5G communication, especially for

The associate editor coordinating the review of this manuscript and approving it for publication was Mengmeng Li.

the critical 5G sub-6 GHz band N78 from 3.3 to 3.8 GHz. Therefore, it is necessary to design a wider bandwidth antenna to cover up to 4 GHz.

For electrically downtilt antenna applications, RF phase shift system is important, which determines the quality of the electrically downtilt function. The works in [8], [9] realize the different phase differences between three channels by switching the current path of the second channel. The phase shift systems only have a few fixed operating modes and cannot shift phase continuously. The design complexity of the feeding network is an issue if the number of current paths is increased. In [10], a five-channel phase shifter is designed to mechanically shift phase continuously. It is more flexible than the phase shift systems in [8], [9]. Compared with the works in [8]–[10], phase shifter based on metamaterial transmission lines (MMLs) can effectively reduce the fluctuation of phase difference with frequency [11]. However, the phase shift range and accuracy of the phase shifter can still have room to improve. In addition, the above modules can only adjust the signal's phase, not the amplitude. Overall, the current solutions are still not enough to meet the performance, cost-effective and ease of implementation requirements of the communication system.

In this paper, a wideband dual-polarized antenna element and its array with a six-channel RF phase shifting module (RFPSM) are designed and analyzed for 4G and 5G communication applications. The antenna element consists a pair of opened-loop dipoles as the fundamental radiator to create dual-polarization. By utilizing cross unexcited dipole and etching U-shaped slots, this antenna element can obtain a wide measured bandwidth of 75.9% from 1.8 to 4 GHz (SWR $\leq$ 2) and high port-to-port isolation of greater than 25 dB. Moreover, with a planar reflector, it achieves a high gain of 8.5 $\pm$ 1 dBi and cross polarization discrimination (XPD) of greater than 20 dB across the whole operation band. Furthermore, a six-element antenna array with electrically downtilt is developed. The gain of the array is enhanced to 15.6 $\pm$ 1.2 dBi. For the practical application, a six-channel RFPSM with cost-effective vector modulators approach is designed and fabricated to provide phase shifting function. The RFPSM can cover the supported frequency bands of the antenna with continuous phase shift from 0 to 360 degree. Finally, by employing a six-channel RFPSM, the antenna array can achieve electrically downtilt from 0° to 12° in V-plane.

II. GEOMETRY OF ANTENNA AND RFPSM

Fig. 1 illustrates the geometry of the proposed dual-polarized antenna element. In order to describe the antenna conveniently, the xoz-plane and yoz-plane are defined as the horizontal plane (H-plane) and the vertical plane (V-plane), respectively. The proposed antenna element, basically, is composed of two cross opened-loop dipoles, two feeding structures, 4 U-shaped slots and a planar reflector. The cross opened-loop dipoles and U-shaped slots are printed on the bottom layer of a FR4 substrate with a dielectric constant of

TABLE 1. Geometrical parameters.

Parameters	L	H	G	S1	S2	R
Value(mm)	25.2	28	78	3.6	0.4	0.26
Parameters	L1	L2	L3	L4	L5	L6
Value(mm)	3.0	9.0	6.5	9.0	7.0	1.7
Parameters	L7	L8	W1	W2	W3	W4
Value(mm)	14.4	6	7.0	2.2	0.54	3.2
Parameters	W5	W6	WG	H_d		
Value(mm)	0.8	4.8	85.6	1.5		

$\varepsilon_r = 4.4$, a loss tangent of 0.02, and a thickness of $H_d = 1.5$ mm. Meanwhile, two feeding structures are printed on the top layer of the substrate. Each dipole is fed by a coaxial cable, and the outer conductor of the cable is connected to an arm of dipole whereas the inner conductor is extended through the substrate and connected to its relative feeding structure to coupled-fed another arm of dipole. The feeding structure of dipole 1 is the simple planar stub structure as shown in Fig. 1. And to avoid overlap, the feeding structure of dipole 2 needs to be designed like a bridge, including top layer stub, two metal vias and bottom layer conductive line *L8* [12]. A U-shaped slot is etched on each arm to improve input impedance matching of the antenna element. For obtaining a unidirectional radiation, a square-shaped plane reflector is employed with a distance of $H = 28$ mm (about 0.25 $\lambda 0$, where $\lambda 0$ is the free-space wavelength at 2.8 GHz). The detailed dimensions of the antenna element are shown in Table 1. After the antenna element is well designed, a six-element array with larger reflector ground plane is developed as shown in Fig. 2. As the antenna part of the electrically downtilt system, the array achieves desired gain, radiation pattern and other performances. The distance between the elements is selected to be 85.6 mm (*WG*, approximately 0.8 λ_0, similar as previous published arts) and the total size of the array is $603 \times 156 \times 28$ mm^3.

In order to realize electrically downtilt function of the antenna array, a six-channel RFPSM is designed, and it is composed of low noise amplifiers (LNA), vector modulators (VM) and a six-channel power combiner. Fig. 3 shows the block diagram of the RFPSM built on a 1.2-mm-thick FR-4 dielectric substrate ($\varepsilon_r = 4.4$). LNA is used to amplify the received single from antenna. VM, known as quadrature or I/Q modulator (TI TRF370317), can adjust the amplitude and phase of the received RF signal by fading its I/Q channel amplitude [13]–[15]. Three two-to-one power combiners and a three-to-one power combiner cascade into a six-channel power combiner. In order to realize broadband, the combiners adopt two-stage structure.

When the RFPSM works, a microcontroller unit (MCU) converts the control signal from computer to the serial peripheral interface (SPI) message, which is routed to a 12 bit eight-channel DAC (TI DAC60508) to create differential V_I and V_Q to fade VMs's I/Q channel signals. The VM output a RF signal whose amplitude and phase is offset by a fix

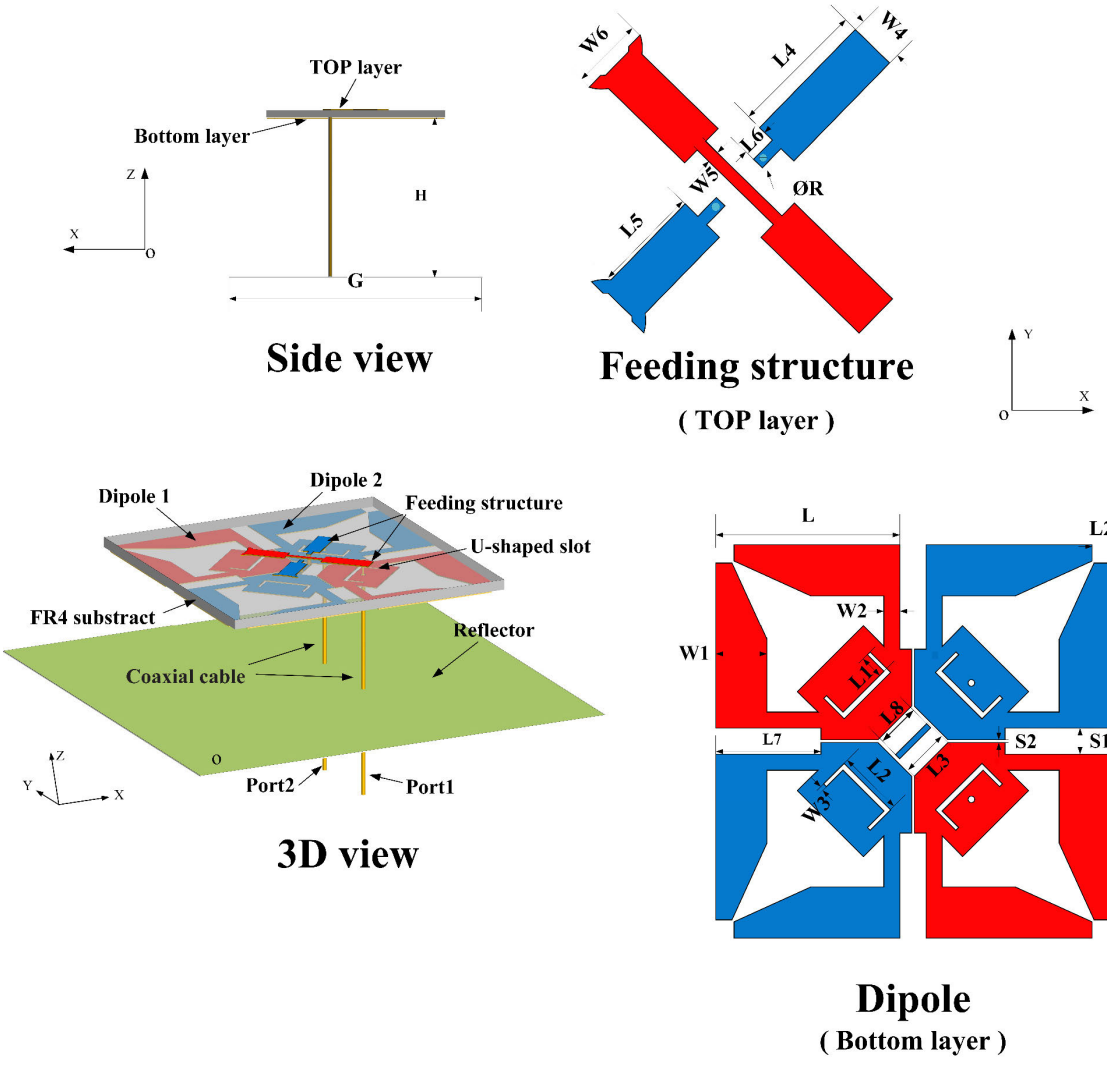

FIGURE 1. Geometry of the antenna element.

value relative to input RF signal. Six VM's output signals are synthesized into an output signal by a six-channel combiner. Theoretically, the phase shift value of the module ranges from 0 to 360 degree, and the precision is affected by the resolution of DAC. In general, the VM-based phase shift system has decent performance and is cost-effective in comparison with phase shifter designs. The proposed antenna array connected with RFPSM can realize electrically downtilt function.

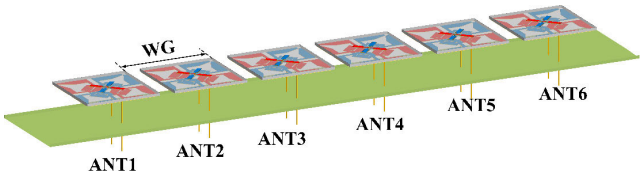

FIGURE 2. 3D view of six-element antenna array.

III. PRINCIPLE OF ANTENNA

To better understand the working mechanisms of the antenna. Key models and dimensions are studied via simulation with Computer Simulation Technology (*CST*) when dipole 1 is excited and dipole 2 is terminated with 50 Ohm load.

A. EFFECT OF PARASITIC RESONATOR

In [16], a principle is described, which is that for a pair of cross dipoles, when the one is driven and the other works as a parasitic resonator, the high order resonant modes of the driven one can be shifted to lower frequency towards its low order resonant modes. When low and high resonant modes are combined together, a wide impedance bandwidth is achieved. The antennas described in [1]–[7] adopt this principle, but they only use two inherent resonant modes of dipole, making it impossible to achieve enough operating bandwidth (covering LTE and 5G sub-6 GHz) to meet the needs for global future communication.

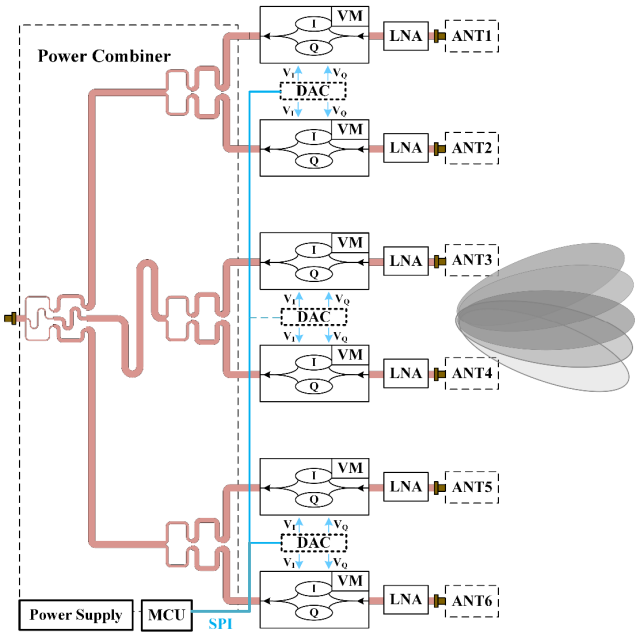

FIGURE 3. Block diagram of RFPSM.

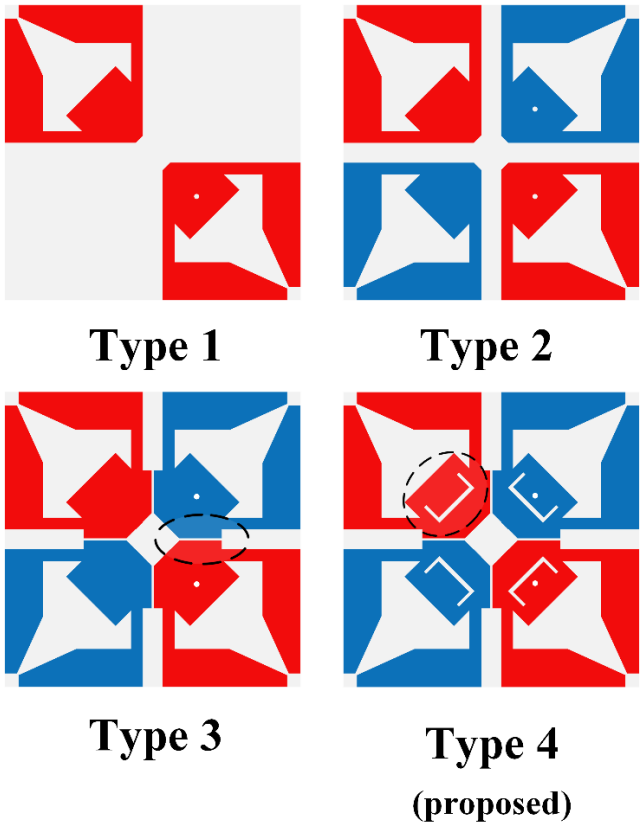

FIGURE 4. Evolution of the proposed antenna models: Type 1, Type 2, Type 3, and Type 4.

The proposed antenna uses three resonant modes to extend the bandwidth. Fig. 4 shows the evolution of the antenna models (i.e., Type 1, Type 2, Type 3, and Type 4). The return loss

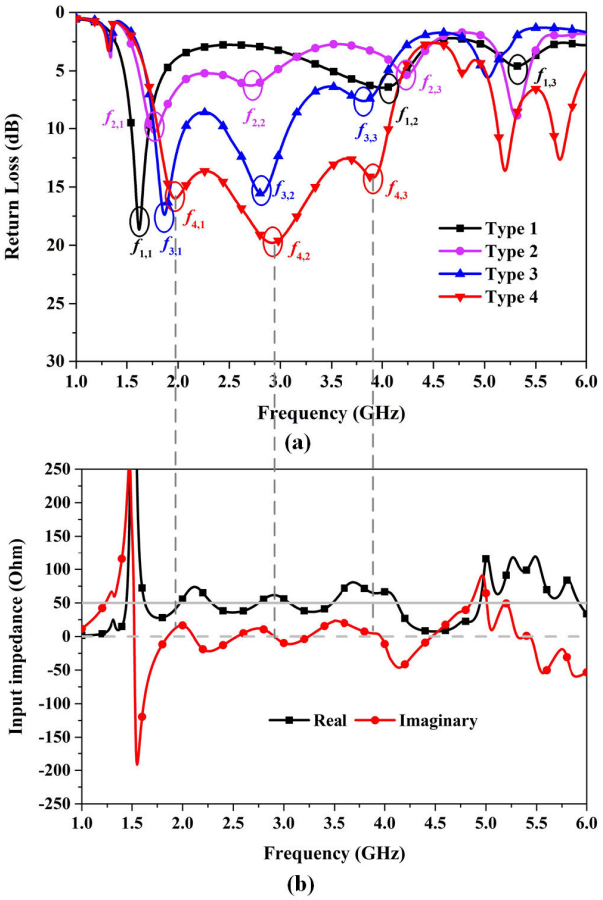

FIGURE 5. Simulated results: (a) return loss of four types; (b) input impedance of Type 4.

of dipole 1 in four models are described in Fig. 5(a). f is the frequency corresponding to the resonant mode. For example, $f_{N,M}$ is the frequency corresponding to the M-th resonant mode in Type N. It can be seen that the dipole 1 in Type 1 owns three resonant modes from 1 to 6 GHz, namely $f_{1,1}$, $f_{1,2}$, $f_{1,3}$. Because the three resonant modes are scattered in the spectrum, the dipole cannot get a wide bandwidth. Based on the above principle [16], Type 2 is designed. It can be obtained from the return loss of Type 2 that after the parasitic resonator (dipole 2) is added, the second and third resonant modes are shifted to the low frequency band. The first resonant frequency moves slightly towards high frequency band and is close to the second resonant mode, but $f_{2,3}$ is still far away from $f_{2,1}$ and $f_{2,2}$. To further enhance the coupling of the parasitic resonator to dipole 1, the antenna adopts ladder-shaped gap for Type 3. Three available resonant modes of Type 3 are close to each other, evenly distributed in 1.5 to 4 GHz. In order to achieve good broadband input impedance matching, Type 3 is improved into Type 4 (proposed antenna) by etching U-shaped slots. Type 4's resonant frequencies $f_{4,1}$, $f_{4,2}$ and $f_{4,3}$ are located at 1.9, 2.8 and 3.9 GHz, respectively. Fig. 5(b) depicts the input impedance of Type 4. The real part of the input impedance of Type 4 fluctuates around 50 Ohm,

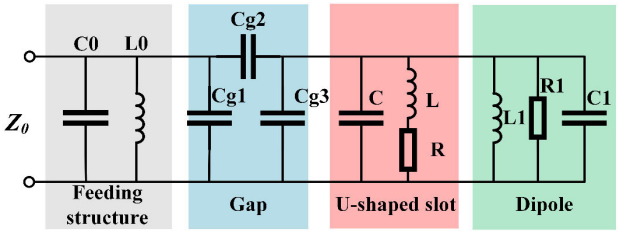

FIGURE 6. Equivalent circuit of the proposed antenna element.

and the imaginary part tightens to 0 Ohm in the full band from 1.8 to 4 GHz. As a result, the proposed antenna based on Type 4 achieves a wide operating bandwidth.

B. EFFECT OF U-SHAPED SLOT

Based on works in [17]–[21], the equivalent circuit of the proposed antenna is shown in Fig. 6. The feeding structure is equivalent to *C0//L0*. A gap between feeding structure and opened-loop dipole is expressed as a Π-type network with three capacitances *Cg1*, *Cg2*, and *Cg3*. The opened-loop dipole is introduced as *L1//R1//C1*. The structure of the U- shaped slot etched around the feed point of dipole 1 is shown in Fig. 1. It is modeled as *C//RL* in the equivalent circuit. Its equivalent impedance (Z_u) can be described as

$$\frac{1}{Zu} = \frac{1}{j\omega L + R} + j\omega C \tag{1}$$

From the above equation, it can be seen that the impedance of the slot is inductive in low frequency and capacitive in high frequency, f_0 is the transition point of reactance.

$$f0 = \frac{1}{2\pi} * \sqrt{\frac{1}{LC} - \frac{R2}{L2}} \tag{2}$$

L1, the length of the U-shaped slot along the current path, is the first important parameter. Fig. 8 shows the effect of *L1* on the input impedance (Z_1) of the proposed antenna, and $f_0$3.3 GHz. It can be observed that when $L1 = 0$ mm (without the U-shaped slot), the absolute value of Z_1 in imaginary part is large in the full band, capacitive reactance in low frequency and inductive in high frequency. As the slot is etched (*L1*> 0 mm) and the length is increased, the capacitive reactance of Z_1 in low frequency decreases while inductive reactance in high frequency continuous to decreases. Therefore, the absolute value of the imaginary part continues to approach zero as shown in the full band, especially in high frequency. The effects of the slot on VSWR are depicted in Fig. 7. It can be seen that when $L1 = 3$ mm, the input impedance matches very well to 50 Ohm in the full band from 1.8 to 4.0 GHz.

C. EFFECT OF OPENED-LOOP DIPOLE

Two simplified models (i.e., closed-loop dipole and opened-loop dipole), which can be seen in Fig. 9, are built to verify the effect of the opened-loop of the proposed antenna. For closed-loop dipole, the gain at 4 GHz drops more than 3 dB from the peak gain at 2.6 GHz. It can be observed that opening

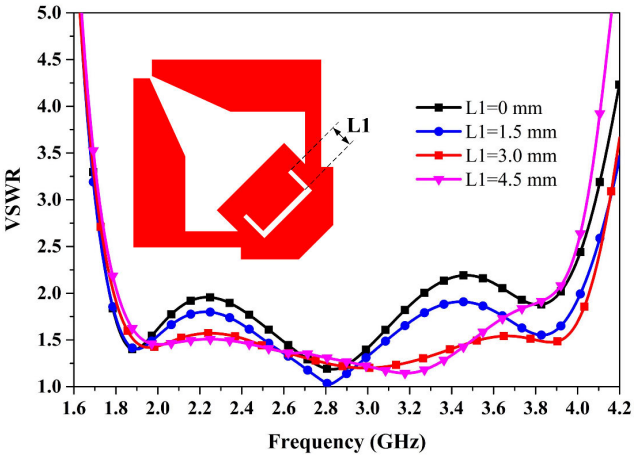

FIGURE 7. Effect of L1 on VSWR.

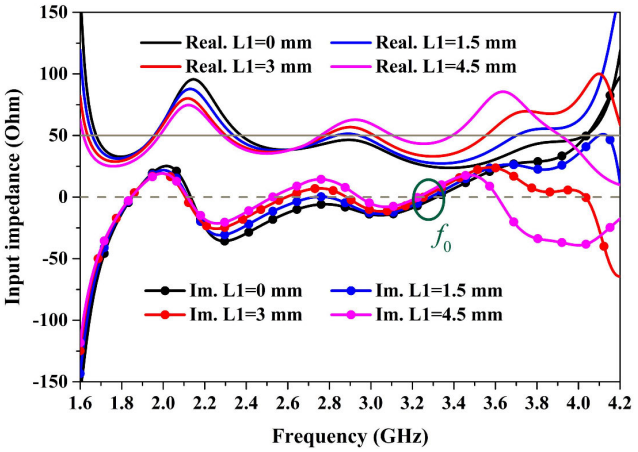

FIGURE 8. Effect of L1 on input impedance.

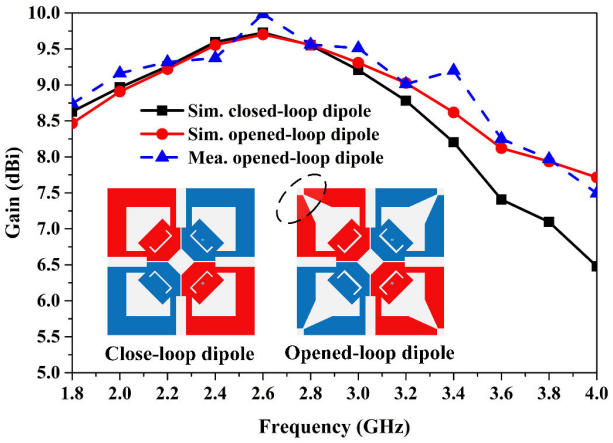

FIGURE 9. Effect of different types on gain.

the end of the closed-loop dipole (high impedance point) can reduce the gain unevenness cross all the bands of interest. As observed in Fig. 9, the gain of the opened-loop dipole is increased by more than 1 dB in high frequency band and the

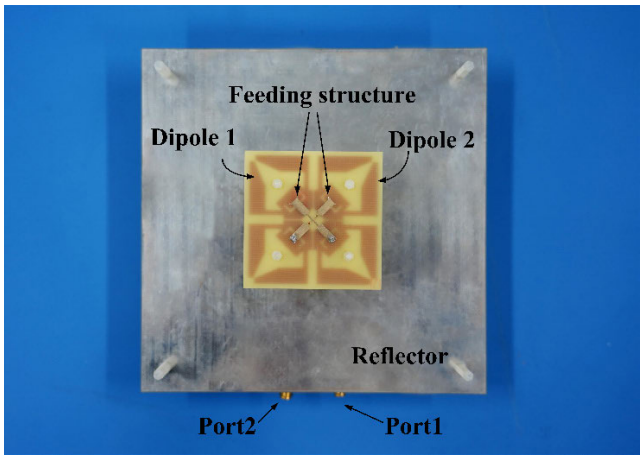

(a)

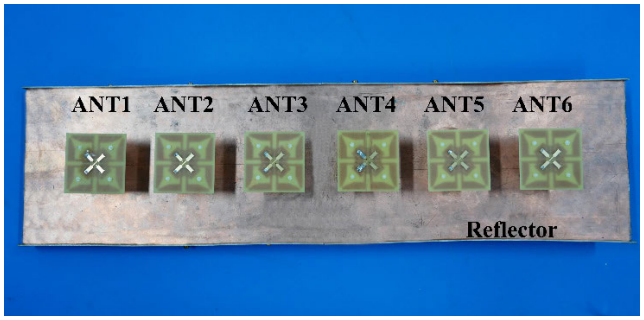

(b)

FIGURE 10. Photos of the antenna element and its six – element array.

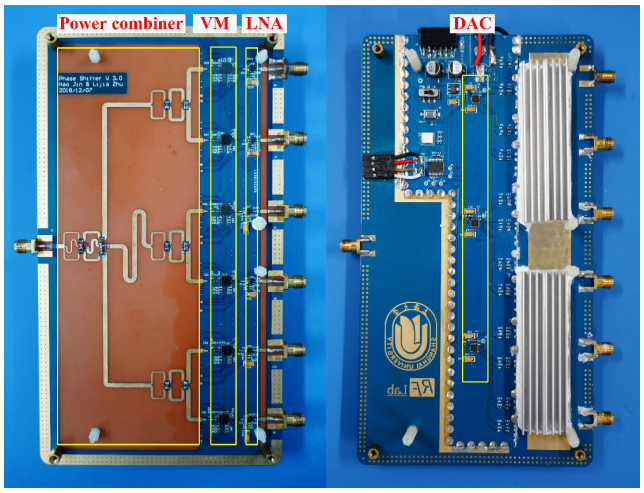

(a) (b)

FIGURE 11. Photos of RFPSM: (a) Top layer, (b) Bottom layer.

gain unevenness is effectively improved. The simulated gain of antenna element is 8.7 ± 1 dBi.

IV. RESULT

To measure the antenna element and its array with electrically downtilt, their prototypes are fabricated in Fig. 10 and RFPSM circuit board is built in Fig. 11. The S - parameters

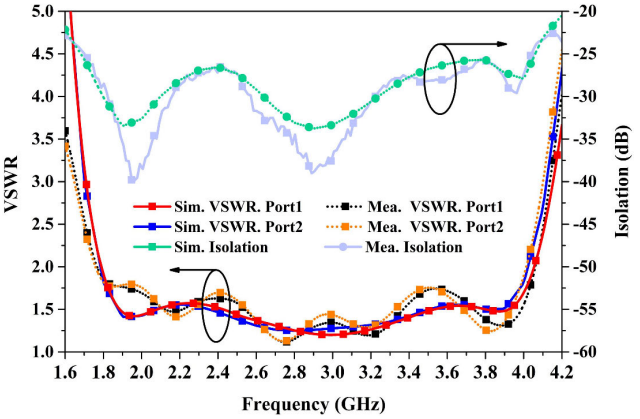

FIGURE 12. Measured VSWR and port-to-port isolation of the antenna element.

TABLE 2. HPBWs of the antenna element.

Frequency (GHz)	H-plane (degree)		V-plane (degree)	
	Sim	Mea	Sim	Mea
1.8	66.7	66	66.4	65.5
2.8	61	66.5	62	66
3.8	68.8	68	70.8	72

TABLE 3. Measured HPBWs of the antenna array.

Downtilt (degree)	H-plane (degree)	V-plane (degree)
0	62.5±6.5	14±3
6	61±3	12.5±2.5
12	57.2±4.2	11.5±2.5

of the antenna are measured by Agilent's vector network analyzer (E5071C). The radiation pattern's raw data (vertical and horizontal) is measured by ETS AMS 8500 chamber, and based on that, the ± 45° slant polarized radiation pattern can be calculated from the equations (3)-(6).

Fig. 12 shows the simulated and measured VSWR and port-to-port isolation of the antenna element. It can be found that the measured results are basically consistent with the simulated results. The measured impedance bandwidth of dipole 1 is 75.9% with VSWR< 2 from 1.8 to 4.0 GHz, while the port-to-port isolation is greater than 25 dB. Fig. 15 shows the VSWR and isolation of the array, the similar as the antenna element. Since the desired patterns cannot be measured directly in a chamber, it needs to be obtained through a series of calculations. Taking the measured pattern of the element at 1.8 GHz as an example, the horizontal and vertical components of the gain can be obtained directly as G_h and G_v, respectively [10].

$$E_h = \sqrt{(Gh * 2\eta)}/4\pi = \sqrt{Gh * 60} \quad (3)$$

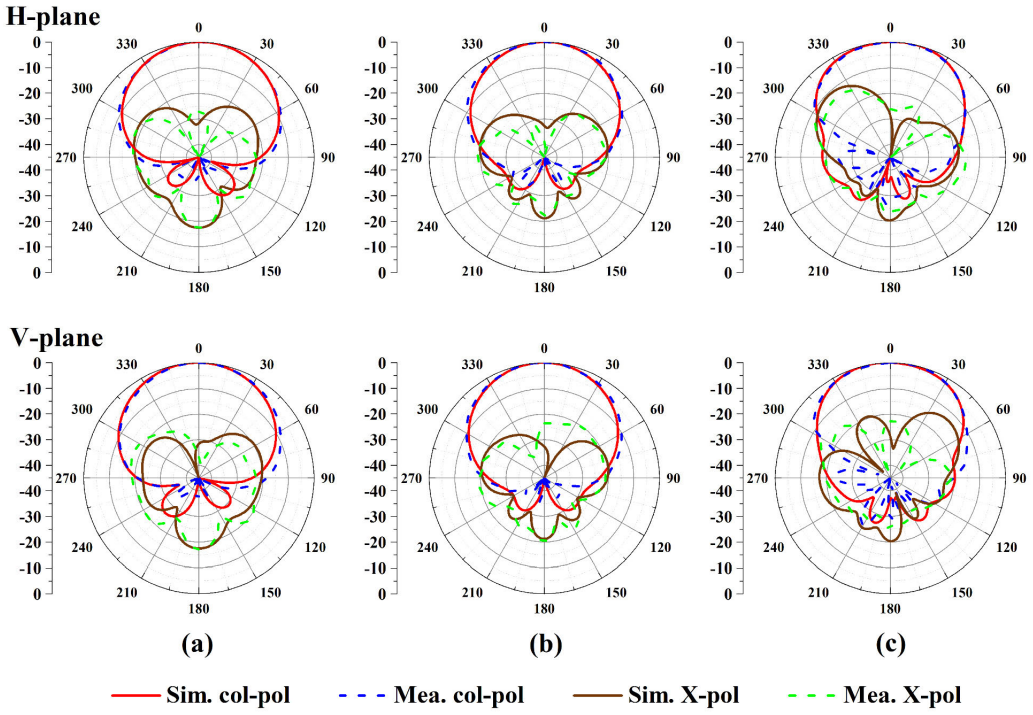

FIGURE 13. Simulated and measured patterns of the antenna element at (a) 1.8, (b) 2.8, (c) 3.8 GHz.

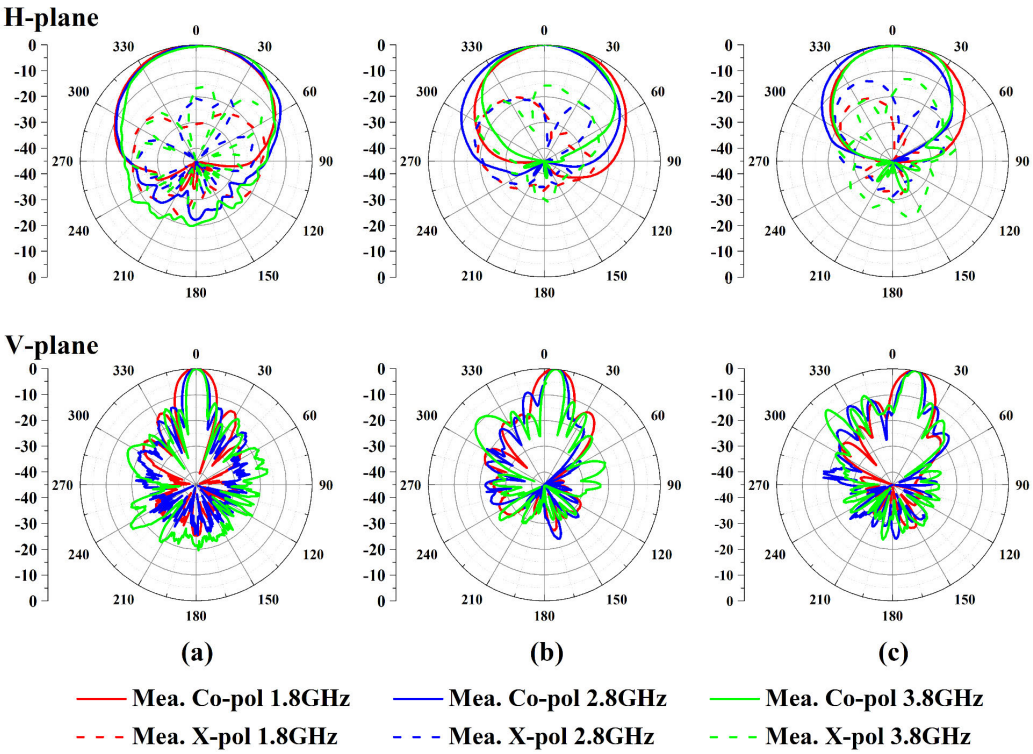

FIGURE 14. Measured patterns of the antenna array with (a) 0°, (b) 6°, (c) 12° electrically downtilt.

$$\mathrm{Ev} = \sqrt{(G\mathrm{v} * 2\eta)}\big/4\pi = \sqrt{G\mathrm{h} * 60} \tag{4}$$

The electric field $\mathrm{E_h}$ and $\mathrm{E_v}$, corresponding to $\mathrm{G_h}$ and $\mathrm{G_v}$, respectively, can be calculated according to formula (3) and (4). And then the ± 45° slant polarized component can be described as

$$|E + 45°| = (|E\mathrm{h}| + |E\mathrm{v}|)\big/\sqrt{2} \tag{5}$$

TABLE 4. Comparison of several antenna elements.

Refs.	Bandwidth	Isolation (dB)	Gain (dBi)	H-plane HPBW (degree)	Element efficiency	Array efficiency
[1]	48% (1.68-2.74 GHz)	> 35	~ 7.9	70±4	NG	NG
[2]	54.5% (1.68-2.94 GHz)	> 28.5	8.5±0.9	66.2±3.7	NG	NG
[3]	52% (1.7-2.9 GHz)	> 26.3	~ 8.5	66.22±3.77	NG	NG
[4]	56.5% (1.66-2.97 GHz)	> 25	~8.2	75±3	NG	NG
[5]	51% (1.68-2.83 GHz)	> 27	8.9±0.5	65.4±2.4	NG	NG
[6]	67.3% (1.4-2.82 GHz)	> 38	8.9±0.7	64.5±4.5	NG	NG
[7]	62% (1.645-3.13 GHz)	> 30	8.5±0.7	NG	NG	NG
[22]	39.6% (0.77-1.15 GHz) (B1) 55.3% (1.66-2.93 GHz) (B2)	> 20	~2.65 (B1) ~4.4 (B2)	NG	~ 80.5% (B1) (Mea) ~ 84.5% (B2) (Mea)	NG
[23]	20.8% (3.10-3.80 GHz)	> 43	>8.1	64±3	~ 83% (Mea)	NG
[24]	55.3% (1.66-2.93 GHz)	> 39	8.6 ± 0.6	68.5±5	~ 83% (Mea)	NG
[25]	38.7% (1.69-2.5 GHz)	> 35	NG	NG	~ 87.7% (Mea)	NG
[26]	30.7% (0.704-0.96 GHz) (B1) 48.2% (1.71-2.69 GHz) (B2)	> 27.5	~ 8.4 (B1) ~ 8.7 (B2)	~ 61.5 (B1) ~ 90 (B2)	~ 84% (B1) (Mea) ~ 85% (B2) (Mea)	~ 88% (B1) (Sim) ~ 91% (B2) (Sim)
This work	**75.9% (1.8-4.0 GHz)**	**> 25**	**8.5±1**	**67±1**	**~ 84% (Mea)**	**~83.6% (Sim)**

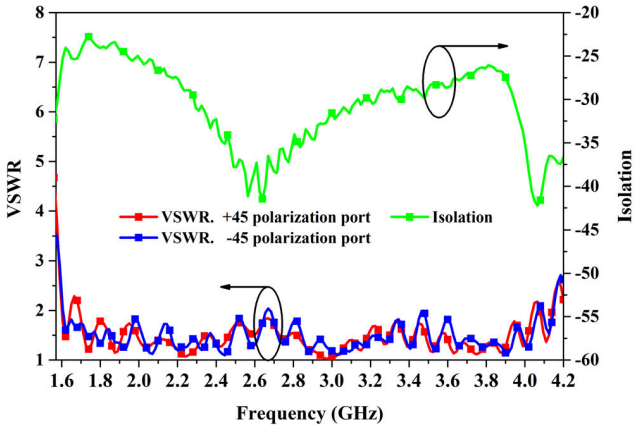

FIGURE 15. Measured VSWR and port-to-port isolation of the antenna array.

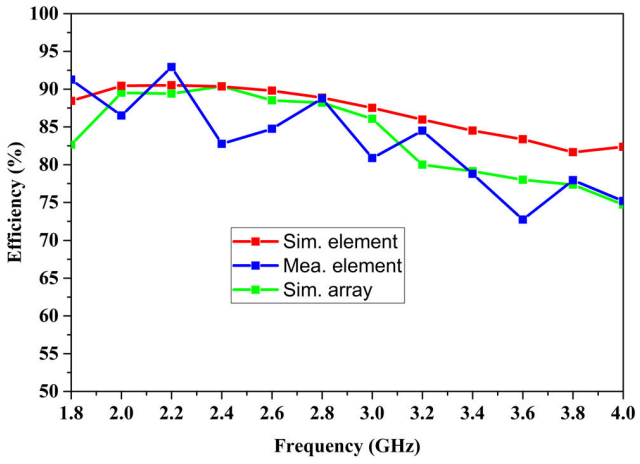

FIGURE 16. Measured efficiency of the antenna.

$$|E-45^{\circ}| = ||Eh| - |Ev||\Big/\sqrt{2} \tag{6}$$

Finally, $G_{+45^{\circ}}$, $G_{-45^{\circ}}$ can be derived from formula (3) and (4) in a reverse way, and the final measured patterns are obtained in Fig. 13(a).

Fig. 13 shows the normalized simulated and measured radiation patterns of the antenna element at selected frequencies of 1.8, 2.8 and 3.8 GHz. The co-pol pattern has the characters of wide beamwidth, small backside lobe and high XPD in the whole band. Table 2 shows the measured half-power beamwidth (HPBW) of the antenna element at these selected frequencies, about 67 ± 1° in H-plane and 68.7 ± 3.3° in V-plane. The measured efficiency of the antenna element as well as the simulated one are depicted in Fig. 16. It is evident that the proposed antenna element achieves a

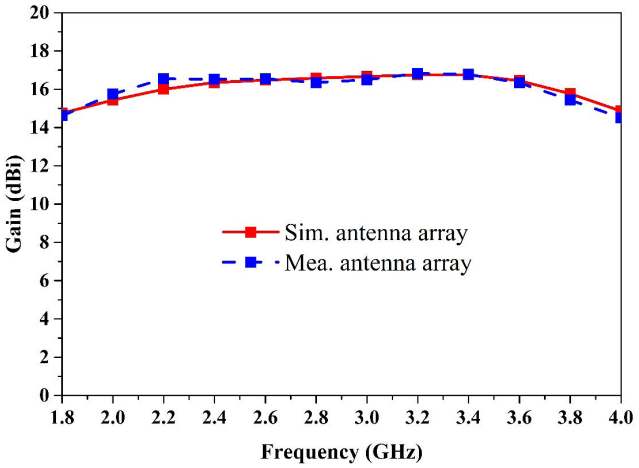

FIGURE 17. Measured and simulated gain of the antenna array without 0° electrically downtilt.

measured average efficiency of 84% within the operating frequency band, which is the similar as that of the other works in [22]–[26]. Due to the loss of the coaxial cables and the SMA connectors, the measured efficiency is lower than the simulated efficiency, especially in high frequency band. The measured gain of the antenna element from 1.8 to 4 GHz is 8.5±1 dBi as shown in Fig. 9. Table 4 compares the performance of the proposed antennas with other antennas. It is found that the proposed antenna element has the advantages of wide bandwidth, high gain and stable pattern. After the antenna element performance is verified, the array with RFPSM is also measured and reported in Fig. 14 and Table 3. The antenna array achieves a simulated average efficiency of 83.6%. Although the simulated average efficiency of the antenna array is slightly lower than that of the work in [26], it is greater than 80% and can meet the efficiency requirement of the base station antenna. In addition, this array has a total measured gain of 15.6 ± 1.2 dBi with 0° electrically downtilt as shown in Fig. 17. Its radiation patterns still achieve a wide beamwidth in the H-plane and the V-plane can be electrically downtilted at the communication normally required angle from 0° to 12°. Table 4 shows the measured HPBW of H-plane and V-plane with 0°, 6°, 12° downtilt. In general, the measured results match fairly well with simulated results for both antenna element and its array, and the differences between simulation and measurement are caused by material and fabrication tolerances.

V. CONCLUSION

A wideband dual-polarized antenna array with a six-channel RF phase shifting module for 4G and 5G sub-6GHz band has been proposed, fabricated and measured. By using the three inherent resonant modes of the opened-loop dipoles and U-shaped slots, the antenna element can obtain a wide impedance bandwidth of 75.9% (VSWR $\leq$ 2) from 1.8 to 4.0 GHz with high port-to-port isolation (> 25 dB) and high XPD (> 20 dB). By adopting two-stage power combiner and cost-effective VM approaches, the electrically downtilt six-element array can maintain 61±8° beamwidth at H-plane and 0° to 12° downtilt in V-plane with a total maximum gain of 16.8 dBi from 1.8 to 4 GHz. In view of these good performances, this antenna array has a great potential for 5G communication and other applications.

REFERENCES

[1] Z. Tang, J. Liu, and Y. Yin, "Enhanced cross-polarization discrimination of wideband differentially fed dual-polarized antenna via a shorting loop," *IEEE Antennas Wireless Propag. Lett.*, vol. 17, no. 8, pp. 1454–1458, Aug. 2018.
[2] D.-Z. Zheng and Q.-X. Chu, "A wideband dual-polarized antenna with two independently controllable resonant modes and its array for base-station applications," *IEEE Antennas Wireless Propag. Lett.*, vol. 16, pp. 2014–2017, 2017.
[3] D.-L. Wen, D.-Z. Dong, and Q.-X. Chu, "A wideband differentially fed dual-polarized antenna with stable radiation pattern for base stations," *IEEE Trans. Antennas Propag.*, vol. 65, no. 5, pp. 2248–2255, May 2017.
[4] Y. Chen, W. Lin, S. Li, and A. Raza, "A broadband ±45° dual-polarized multidipole antenna fed by capacitive coupling," *IEEE Trans. Antennas Propag.*, vol. 66, no. 5, pp. 2644–2649, May 2018.
[5] D. Zheng and Q. Chu, "A multimode wideband ±45° dual-polarized antenna with embedded loops," *IEEE Antennas Wireless Propag. Lett.*, vol. 16, pp. 633–636, 2017.
[6] S. Fu, Z. Cao, P. Chen, D. Gao, and X. Quan, "A novel bandwidth-enhanced dual-polarized antenna with symmetrical closed-resonant-slot pairs," *IEEE Access*, vol. 7, pp. 87943–87950, 2019.
[7] J.-H. Xun, L.-F. Shi, W.-R. Liu, G.-X. Liu, and S. Chen, "Broadband dual-polarised antenna with wideband decoupling structure for polarisation diversity wireless communication application," *IET Microw. Antennas Propag*, vol. 13, no. 7, pp. 917–925, Jun. 2019.
[8] L. Ge and K. M. Luk, "A three-element linear magneto-electric dipole array with beamwidth reconfiguration," *IEEE Antennas Wireless Propag. Lett.*, vol. 14, pp. 28–31, 2015.
[9] B. Feng, Y. Tu, K. L. Chung, and Q. Zeng, "A beamwidth reconfigurable antenna array with triple dual-polarized magneto-electric dipole elements," *IEEE Access*, vol. 6, pp. 36083–36091, 2018.
[10] D.-L. Wen, D.-Z. Zheng, and Q.-X. Chu, "A dual-polarized planar antenna using four folded dipoles and its array for base stations," *IEEE Trans. Antennas Propag.*, vol. 64, no. 12, pp. 5536–5542, Dec. 2016.
[11] K. L. Chung, "High-performance circularly polarized antenna array using metamaterial-line based feed network," *IEEE Trans. Antennas Propag.*, vol. 61, no. 12, pp. 6233–6237, Dec. 2013.
[12] Y. Cui, X. Gao, H. Fu, Q.-X. Chu, and R. Li, "Broadband dual-polarized dual-dipole planar antennas: Analysis, design, and application for base stations," *IEEE Antennas Propag. Mag.*, vol. 59, no. 6, pp. 77–87, Dec. 2017.
[13] Z. Peng, J. Chen, Y. Dong, B. Zhang, S. Qiao, D. Ye, J. Huangfu, Y. Sun, C. Li, and L. Ran, "Radio frequency beamforming based on a complex domain frontend," *IEEE Trans. Microw. Theory Techn.*, vol. 64, no. 1, pp. 289–298, Jan. 2016.
[14] W. Yang, J. Zhou, K. Zhou, and Z. Yu, "A 5.8-GHz active transmitting array based on frequency shiftable vector modulator module," *IEEE Antennas Wireless Propag. Lett.*, vol. 15, pp. 1085–1088, 2016.
[15] F. Hutu, D. Cordeau, and J.-M. Paillot, "2.4 GHz antenna array using vector modulatorbased active phase shifters for beamforming," *IET Microw., Antennas Propag.*, vol. 5, no. 2, pp. 245–254, Jan. 2011.
[16] Q. Chu, D. Wen, and Y. Luo, "Principle of multimode broadband antennas with resonator-loaded dipole," presented at the Int. Workshop Antenna Technol. (iWAT), Seoul, South Korea, Mar. 2015.
[17] J.-D. Zhang, L. Zhu, Q.-S. Wu, N.-W. Liu, and W. Wu, "A compact microstrip-fed patch antenna with enhanced bandwidth and harmonic suppression," *IEEE Trans. Antennas Propag.*, vol. 64, no. 12, pp. 5030–5037, Dec. 2016.
[18] Y. Liao, X. Ying, G. Shi, and Y. Wang, "Time domain response analysis with equivalent circuit models for dipole antennas under EMP," presented at the 6th IEEE Int. Symp. Microw., Antenna, Propag., EMC Technol. (MAPE), Shanghai, China, Oct. 2015.
[19] C.-T. Chuang and S.-J. Chung, "Synthesis and design of a new printed filtering antenna," *IEEE Trans. Antennas Propag.*, vol. 59, no. 3, pp. 1036–1042, Mar. 2011.

[20] C.-K. Lin and S.-J. Chung, "A compact filtering microstrip antenna with quasi-elliptic broadside antenna gain response," *IEEE Antenna Wireless Propag. Lett.*, vol. 10, pp. 381–384, 2011.
[21] Z. Abbasi, P. Shariaty, M. Nosrati, Z. Hashisho, and M. Daneshmand, "Dual-band microwave circuits for selective binary gas sensing system," *IEEE Trans. Microw. Theory Techn.*, vol. 67, no. 10, pp. 4206–4219, Oct. 2019, doi: 10.1109/TMTT.2019.2934459.
[22] Z. Zhao, J. Lai, B. Feng, and C.-Y.-D. Sim, "A dual-polarized dual-band antenna with high gain for 2G/3G/LTE indoor communications," *IEEE Access*, vol. 6, pp. 61623–61632, 2018.
[23] Y. Liu, S. Wang, X. Wang, and Y. Jia, "A differentially fed dual-polarized slot antenna with high isolation and low profile for base station application," *IEEE Antennas Wireless Propag. Lett.*, vol. 18, no. 2, pp. 303–307, Feb. 2019.
[24] Z. Zhou, Z. Wei, Z. Tang, Y. Yin, and J. Ren, "Compact and wideband differentially fed dual-polarized antenna with high common-mode suppression," *IEEE Access*, vol. 7, pp. 108818–108826, 2019.
[25] R. Lian, Z. Wang, Y. Yin, J. Wu, and X. Song, "Design of a low-profile dual-polarized stepped slot antenna array for base station," *IEEE Antennas Wireless Propag. Lett.*, vol. 15, pp. 362–365, 2016.
[26] H. Huang, Y. Liu, and S. Gong, "A dual-broadband, dual-polarized base station antenna for 2G/3G/4G applications," *IEEE Antennas Wireless Propag. Lett.*, vol. 16, pp. 1111–1114, 2017.

HAO JIN was born in Shanxi, China, in 1995. He received the B.S. degree in electronic science and technology from the Shanghai University of Electric Power, Shanghai, China, in 2017. He is currently pursuing the M.S. degree in electromagnetic fields and microwave technology with Shanghai University, China.

His main research interests include dual-polarized antenna array, cost-effective RF phase shifting module, and communication receiver.

LIJIA ZHU was born in Shanghai, China, in 1994. He received the B.S. degree in communication engineering and the M.S. degree in electromagnetic fields and microwave technology from Shanghai University, Shanghai, China, in 2016 and 2019, respectively.

He joined Texas Instruments as a Senior Field Application Engineer, responsible for high speed signal chain. His main research interests include millimeter-wave antenna array, millimeter-wave short range radar, and communication receiver.

He is currently serving as a Reviewer for the IEEE Antennas and Wireless Propagation Letters and the *Applied Computational Electromagnetics Society Journal*.

HUANQING ZOU was born in Zhejiang, China, in 1990. He is currently pursuing the Ph.D. degree in electromagnetic field and microwave technology with Shanghai University, China.

His main research interests are MIMO antenna arrays, 5G smartphone antennas, multiband antennas, and millimeter-wave antennas.

Mr. Zou serves as a Reviewer for IEEE Access and the *International Journal of RF and Microwave Computer-Aided Engineering*.

YONG LUO received the Ph.D. degree from The University of Tokyo, Tokyo, Japan, in 2015, with a focus on active metamaterials for scanning radiation beams by using micromachining fabrication process to monolithically integrate antenna with MEMS.

From 2010 to 2012, he was an Electrical Engineer with Huawei, Shanghai, China, where he involved in phased array antennas for base stations. He was with Prof. Sievenpiper's Applied Electromagnetic Group, San Diego, CA, USA, where he held a postdoctoral position in the field of nonlinear metasurfaces using diodes, in 2016. He is currently an Assistant Professor with the Department of Electronic and Information Engineering, School of Communication and Information Engineering, Shanghai University, Shanghai. His current research interests include active antennas, nonlinear metamaterial, and RF-MEMS.

SHUGONG XU (M'98–SM'06–F'16) received the B.Sc. degree from Wuhan University, in 1990, and the M.E. and Ph.D. degrees from the Huazhong University of Science and Technology (HUST), in 1993 and 1996, respectively. He is currently a Professor with Shanghai University and the Head of the Shanghai Institute for Advanced Communication and Data Science (SICS). In his 20+ years career in research (more than 15 years in industrial research labs), he has had more than 40 issued U.S./WO/CN patents and published more than 100 peer-reviewed research articles. His work was one of the major triggers of the research and standardization of IEEE 802.11S. His current research interests include wireless communication systems and machine learning. He was named an IEEE Fellow for contributions to the improvement of wireless network efficiency, in 2015 and was awarded the National Innovation Leadership Talent from the China government, in 2013. He also received the 2017 Award for Advances in Communication from IEEE Communications Society.

GUANGLI YANG (M'06) received the B.S. degree in physics from the Beijing University of Science and Technology, Beijing, China, in 1997, and the Ph.D. degree in electrical engineering from the University of South Carolina, Columbia, SC, USA, in 2005.

From 2005 to 2013, he was with the Antenna and RF Research Group, Motorola, Inc., Chicago, IL, USA, where he started as Senior Staff and was then promoted as a Principal Engineer. Since 2014, he has been a Professor with Shanghai University, Shanghai, China, where he is currently the Director of the RF Research Group. He has authored or coauthored more than 60 publications. He holds 21 patents filed or issued. His current research interests include smart antennas, antenna miniaturization and configurability, digital beamforming systems, and microwave circuits.

Dr. Yang was a recipient of the Shanghai Eastern Scholarship Awards, in 2013.